Practical Range Camera Calibration[1]

J.-A. Beraldin, S. F. El-Hakim, and L. Cournoyer
Institute for Information Technology
National Research Council of Canada
Ottawa, Canada K1A 0R6

Abstract

This paper presents a calibration procedure adapted to a range camera intended for space applications. The range camera, which is based upon an auto-synchronized triangulation scheme, can measure objects from about 0.5 m to 100 m. The field of view is 30° × 30°. Objects situated at distances beyond 10 m can be measured with the help of cooperative targets. Such a large volume of measurement presents significant challenges to a precise calibration. A two- step methodology is proposed. In the first step, the close-range volume (from 0.5 m to 1.5 m) is calibrated using an array of targets positioned at known locations in the field of view of the range camera. A large number of targets are evenly spaced in that field of view because this is the region of highest precision. In the second step, several targets are positioned at distances greater than 1.5 m with the help of an accurate theodolite and electronic distance measuring device. This second step will not be discussed fully here. The internal and external parameters of a model of the range camera are extracted with an iterative nonlinear simultaneous least-squares adjustment method. Experimental results obtained for a close-range calibration suggest a precision along the x, y and z axes of 200 μm, 200 μm, and 250 μm, respectively, and a bias of less than 100 μm in all directions.

1   Introduction

In many disciplines of science, there is one that is certainly common to all, that is, the science of measurement, or metrology. As one seeks to measure a physical quantity (variable) either to inform, e.g., temperature, to predict ,e.g., weather patterns, or to give some indication of the validity of a theory, the most accurate data are always sought. One thing must first be defined, that is, what one means by most accurate. For some, it may mean an absolute measurement taken in comparison to some predefined standard. For others, it may just be a relative measurement. The process by which a measurable quantity is obtained should be as free as possible of systematic errors (bias) and should provide the highest level of precision (spread centered around an average value). Usually, these characteristics are also given with some level of confidence, e.g., confidence intervals or probability density functions.

As a technology that encompasses many disciplines of the physical sciences, digital 3-D imaging must also rely upon metrology. Among the many noncontact techniques proposed to extract 3-D information from a scene, active triangulation is used in applications as diverse as measurement and reproduction of objects, inspection of printed circuit boards, and automatic robot welding[1,2,8]. An innovative approach, based on triangulation using a synchronized scanning scheme, was introduced by Rioux[3] to allow very large fields of view with small triangulation angles, without compromising on precision. A 3-D surface map is captured by scanning a laser beam onto a scene along two orthogonal directions. Owing to the shape of the coordinate system spanned by the measured variables, the resultant images are not compatible with coordinate systems used by most geometric image processing algorithms. An unambiguous transformation (one-to-one) or, in other words, a re-mapping of these variables to a more common coordinate system like a rectangular system is therefore required. The process of measuring the original variables to a high level of confidence and the determination of the re-mapping function is known as camera calibration.

This paper presents a calibration procedure adapted to a range camera intended for space applications. With this camera, position and orientation of objects can be measured when they are within a field of view of 30° × 30° and with corresponding range from about 0.5 m to 100 m. Such a large volume of measurement presents significant challenges to a precise calibration. A two-step methodology is proposed to calibrate this range camera at close and far range. The details of the range camera are presented in Section 2. Section 3 highlights the advantages of the synchronized scanning scheme over conventional triangulation. It includes an analytical treatment of the synchronized geometry, where the projective transformation equations of this optical arrangement for single and dual scan axes are presented. These equations are used in Section 4 as design tools to characterize the spatial precision and establish
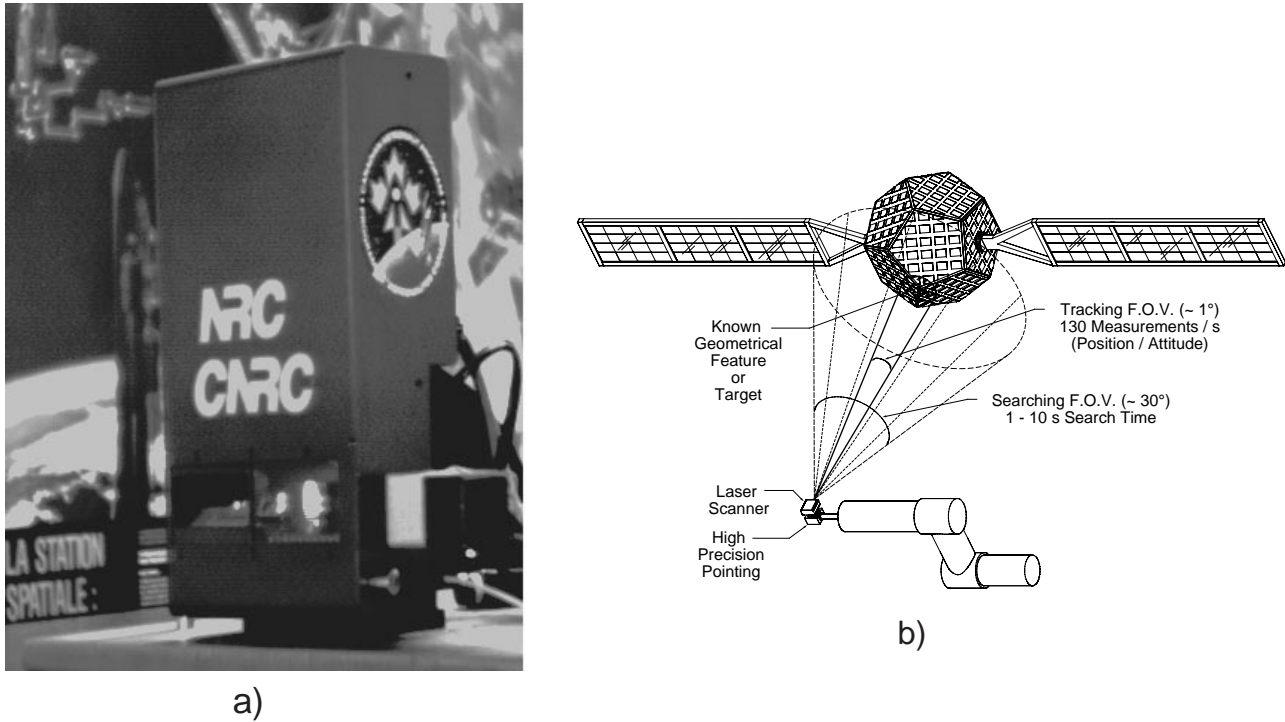

Figure 1: Range camera: (a) photograph, (b) real-time tracking of satellites.

a calibration procedure. The precision and accuracy assessments of the range camera and the proposed calibration method are described in Section 5. Experimental results obtained from a close-range calibration are presented. Finally, a discussion follows in Section 6 of several advantages and limitations of the analysis and of the proposed technique. Conclusions appear in Section 7.

2   Laser Range Camera for Space Applications

The laser range camera is shown in Figure 1a. This range camera can operate in either a variable resolution mode or a raster type mode. In the variable resolution mode, as illustrated in Figure 1b, the laser scanner tracks targets and geometrical features of objects located within a field of view of $30° \times 30°$ and with corresponding range from about 0.5 m to 100 m. For objects located at distances greater than 10 m, cooperative targets on their surfaces are required for good signal-to-noise ratio[4]. The range camera uses two high-speed galvanometers to steer the laser beam to any spatial location within the field of view of the camera. A compact and versatile dual-galvanometer controller was designed specifically for this task. Each axis can be addressed by more than 16 bits with a step response of 1.8 μs over wide angles even though the mirrors are quite large. This increase in speed and versatility over the original manufactured controller allows the generation of Lissajous patterns for tracking of objects at a refresh rate of up to 130 Hz.

The raster mode is used primarily for the measurement of registered range and intensity information of large stationary objects[5]. Figure 2 shows a shaded image of a quarter-scale model (at the National Research Council) of the cargo bay of the Space Shuttle Orbiter. The scale model measures 4.33 m by 1.42 m by 0.6 m. It was digitized to a resolution of 2048 × 4096.

3   Range Camera Equations

3.1   Conventional Active Triangulation

The basic geometrical principle of optical triangulation is shown in Figure 3a. The light beam generated by the laser is deflected by a mirror and scanned on the object. A camera, composed of a lens and a position sensitive photodetector,
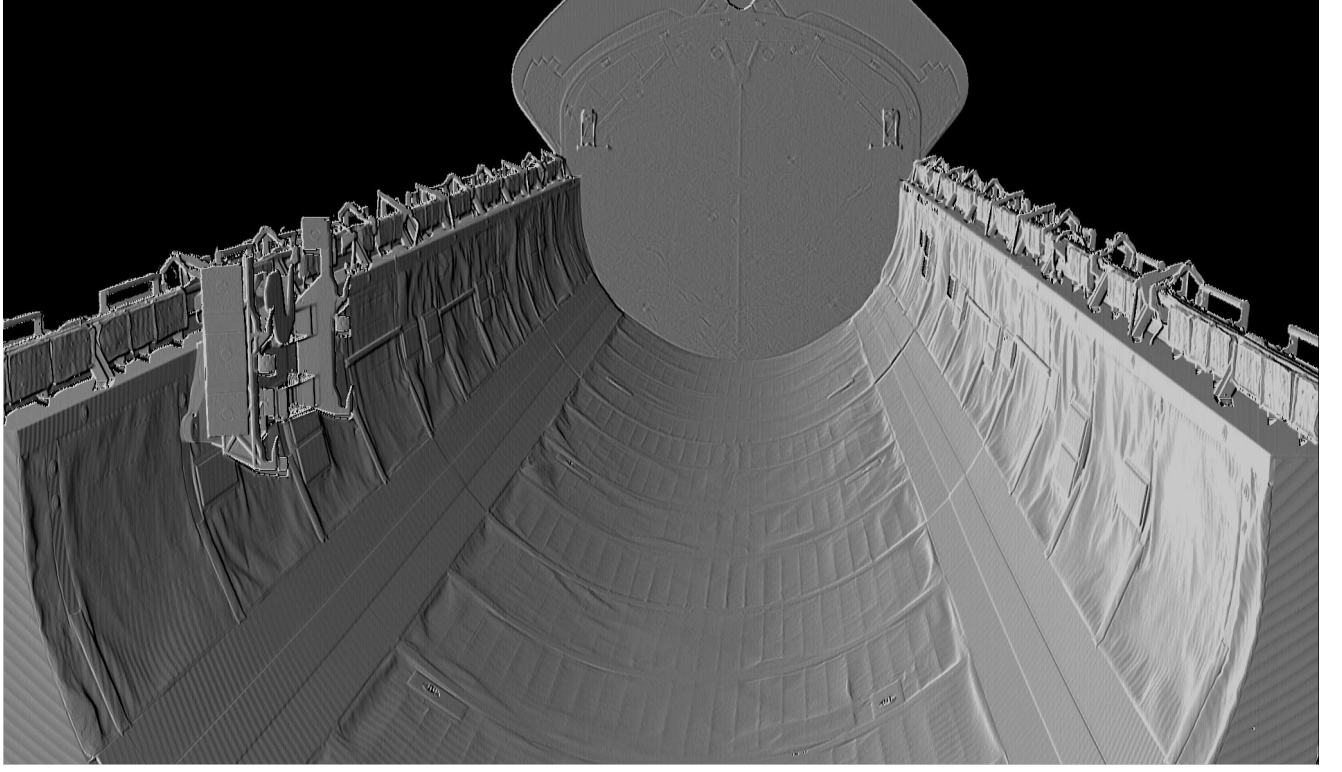
Figure 2: Shaded image of scaled model of cargo bay.

measures the location of the image of the illuminated point on the object. By simple trigonometry, the x, z coordinate of the illuminated point on the object in a rectangular coordinate system is calculated. From Figure 3a,

$$z = \frac{d\,f_0}{p + f_0\,\tan(\theta)} \tag{1}$$

and

$$x = z\,\tan(\theta) \tag{2}$$

where p is the position of the imaged spot on the position detector, θ is the deflection angle of the laser beam, d is the separation between the lens and the laser source, and f_0 is the effective distance between the position detector and the lens. f_0 is related to the focal length of the lens.

To show some of the limitations of this triangulation method, let us approximate the standard deviation of the error in z, σ_z, as a function of p only. The law of propagation of errors gives

$$\sigma_z = \frac{z^2}{f_0\,d}\,\sigma_p \tag{3}$$

where σ_p is the standard deviation of the error in the measurement of p. The error in the estimate of z is therefore inversely proportional to both the separation between the laser and the position detector and the effective position of the lens, but directly proportional to the square of the distance. Unfortunately, f_0 and d cannot be made as large as desired. d is limited mainly by the mechanical structure of the optical setup and by shadow effects. As seen in Figure 3b, d must be kept small to minimize these effects.

In the conventional triangulation geometry, the field of view Φ_x of the sensor, where the light beam can be scanned over the whole field of view, is given approximately by

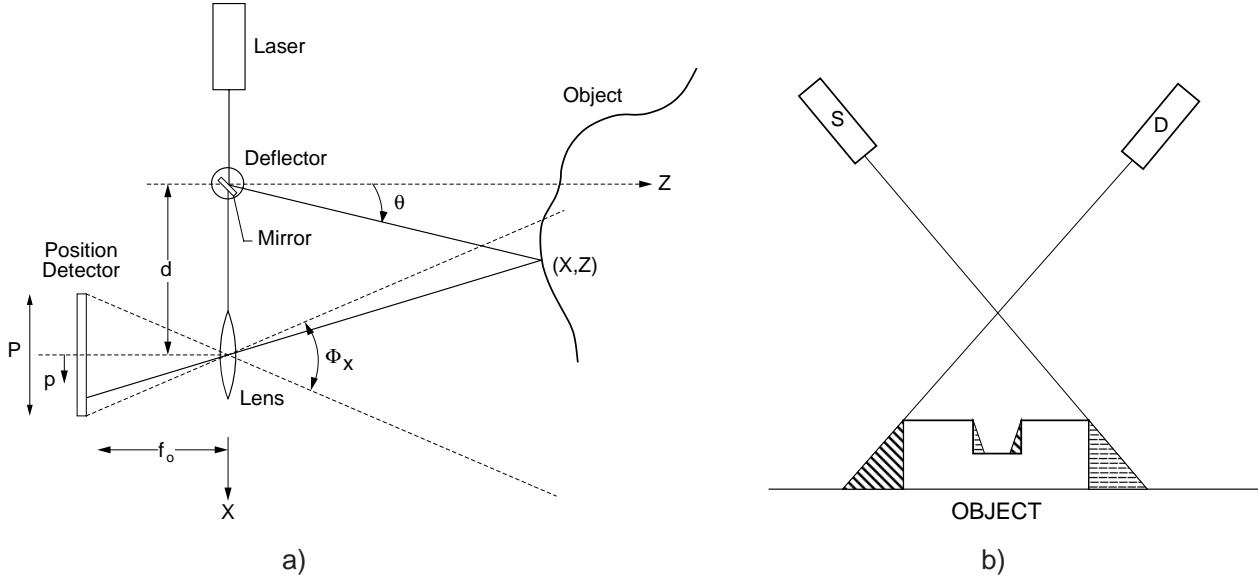$$\Phi_x \approx 2\arctan(\frac{P}{2\,f_0}) \tag{4}$$

Figure 3: Active triangulation from [8]: (a) basic principle, (b) shadow effects.

where P is the length of the position detector. Therefore, in the conventional setup, a compromise between field of view, precision of the 3-D measurement, and shadow effects must be considered.

3.2 Synchronized Scanning

Large fields of view with small triangulation angles can be obtained using synchronized scanner techniques without sacrificing precision. With smaller triangulation angles, a reduction of shadow effects is inherently achieved. The intent is to synchronize the projection of the light spot with its detection. As depicted in Figure 4a, the instantaneous field of view of the position detector follows the spot as it scans the scene. The focal length of the lens is therefore related only to the desired depth of field or measurement range. Rioux[3] introduced an innovative approach, based on such a synchronized scanning scheme. Implementation of this triangulation technique by an auto-synchronized scanner approach allows a considerable reduction in the optical head size compared to conventional triangulation methods (Figure 4b).

Figure 5 depicts schematically the basic components of a dual-axis camera. With such a camera, one captures a 3-D surface map by scanning a laser beam onto a scene by way of two oscillating mirrors, collecting the light that is scattered by the scene in synchronism with the projection mirrors, and, finally, focusing this light onto a linear position detector, e.g., photodiode array, charge-coupled device, or lateral effect photodiode. The image acquisition process yields three quantities per sampling interval: two are for the angular position of the mirrors and one for the position of the laser spot on the position detector. The projective transformation equations of this optical arrangement follow.

3.3 Single Scan Axis Case

Figure 6a shows the geometry used for the triangulation where the projection and collection axes have been unfolded. The dotted lines depict the static geometry, i.e., for $\theta = 0$. The optical angle θ is measured from these dotted lines. Superimposed on this figure is the equivalent geometry for a synchronized rotation of the projection and collection axes by an angle θ. Collinearity equations relate the spot position p to the location of a point on the projection axis. Here, the scanning mirrors have been temporarily removed and a pinhole model for the collecting lens has been assumed. Furthermore, it is assumed that the scanning mirror is thin and flat and that there is no wobble present in the axis of rotation. A rectangular coordinate system has been located on the axis joining the equivalent position of the respective pivot of the projection and collection axes. These two positions are represented by large circles on the X axis. The Z axis extends from a point midway between them toward infinity.

The synchronized geometry implies that, for a spot position $p = 0$ (point **A** on the position detector of Fig. 6a), the acute angle between the projection and collection paths is equal to a constant γ. From this, all other angles can
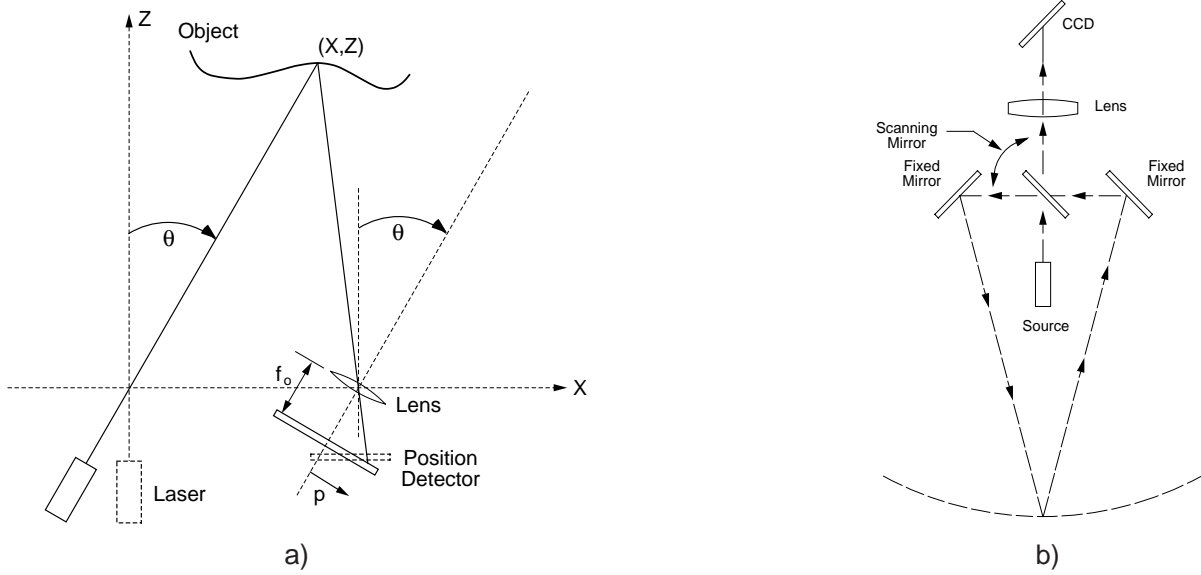
4

Figure 4: Synchronized scanner approach: (a) basic principle, (b) auto-synchronization.

be inferred. Two sets of similar triangles, **OAC–OED** and **OBC–OFD**, can be identified. From these, the following relation is extracted,

$$\frac{R_p(\theta) - R_{-\infty}(\theta)}{R_0(\theta) - R_{-\infty}(\theta)} = \frac{P_\infty}{P_\infty - p} \tag{5}$$

where for a given optical angle θ, $R_p(\theta)$ is the distance $R(\theta)$ along the projection axis corresponding to p, $R_{-\infty}(\theta)$ is the location of the vanishing point on the projection axis, and $R_0(\theta)$ is the location corresponding to $p = 0$. P_∞ is the location of the vanishing point on the detection axis:

$$P_\infty = f_0 \, \frac{\sin(\gamma)}{\cos(\beta - \gamma)} = \frac{(f_0 - f)}{\sin(\beta)} \tag{6}$$

where f is the focal length of the lens, f_0 is the effective distance of the position detector to the imaging lens, β is the tilt angle of the position detector found according to the Scheimpflug condition, and γ is the triangulation angle.

Using the same terminology as in photogrammetry, (5) is designated as the projective transformation equation for this active triangulation method. The collinear transformation equation is found by inverting (5), that is

$$p(R) = P_\infty \left(1 - \frac{R_0(\theta) - R_{-\infty}(\theta)}{R_p(\theta) - R_{-\infty}(\theta)} \right) \tag{7}$$

The transformation of eq. (5) to an X, Z representation is computed from the fact that three points **D**, **E** and **F** belong to the same straight line if the vectors $\vec{\mathbf{DE}}$ and $\vec{\mathbf{DF}}$ are linearly dependent. Hence,

$$\frac{X_p(\theta) - X_{-\infty}(\theta)}{X_0(\theta) - X_{-\infty}(\theta)} = \frac{Z_p(\theta) - Z_{-\infty}(\theta)}{Z_0(\theta) - Z_{-\infty}(\theta)} = \frac{P_\infty}{P_\infty - p} \tag{8}$$

The equation is decomposable in both orthogonal directions, i.e.,

$$x_{\mathrm{s}}(p, \theta) = X_{-\infty}(\theta) + P_\infty \, \frac{X_0(\theta) - X_{-\infty}(\theta)}{P_\infty - p} \tag{9}$$

$$z_{\mathrm{s}}(p, \theta) = Z_{-\infty}(\theta) + P_\infty \, \frac{Z_0(\theta) - Z_{-\infty}(\theta)}{P_\infty - p} \tag{10}$$
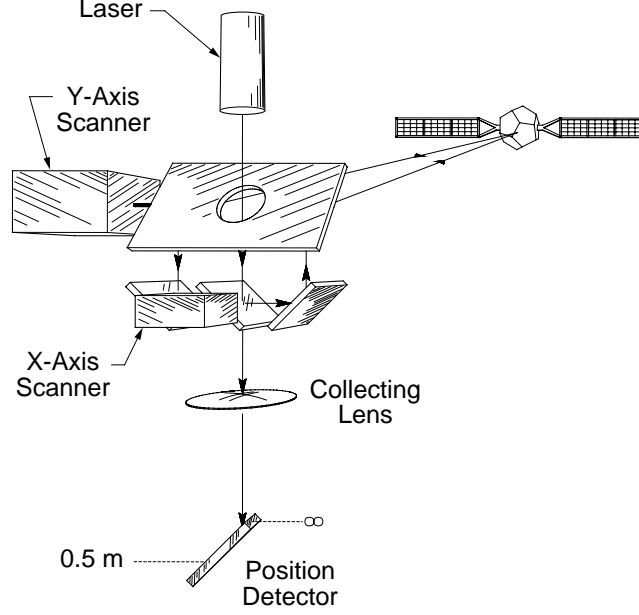
5

Figure 5: Dual-axis synchronized scanner.

The coordinates of points **D**, **E**, and **F** are

$$X_{-\infty}(\theta) \;=\; \frac{T\,\cos(\beta - 2\,\theta) + S\,\cos(\beta)\,\sin(\gamma/2 - \theta)}{\cos(\beta - \gamma)} \tag{11}$$

$$Z_{-\infty}(\theta) \;=\; \frac{S\,\cos(\beta)\,\cos(\gamma/2 - \theta)}{\cos(\beta - \gamma)}$$
$$-\frac{T\,(\sin(\beta - 2\,\theta) + \sin(\beta - \gamma))}{\cos(\beta - \gamma)} \tag{12}$$

$$X_0(\theta) \;=\; T\,\frac{\sin(2\,\theta)}{\sin(\gamma)} \tag{13}$$

$$Z_0(\theta) \;=\; -T\,\frac{\cos(2\,\theta) + \cos(\gamma)}{\sin(\gamma)} \tag{14}$$

where S is the distance between the lens and the effective position of the collection axis pivot and T is half the distance between the projection and collection pivots.

3.4 Dual Scan Axis Case

The second scan axis is implemented as depicted in Figure 6b with a galvanometer driven mirror. Again, it is assumed that the scanning mirror is thin and flat and no wobble is present in the axis of rotation. Moreover, the second scan axis mirror has been mounted orthogonally to the first mirror (x-axis scanner). According to the convention set out in Figure 6b and after some manipulations, the equations of a point (x, y, z) in the camera field of view as a function of (p, θ, ϕ) are

$$x(p, \theta, \phi) \;=\; x_{\mathrm{s}}(p, \theta) \tag{15}$$

$$y(p, \theta, \phi) \;=\; (z_{\mathrm{s}}(p, \theta) \;-\; h_{\mathrm{x}}\cos(\gamma/2) \;-\; h_{\mathrm{y}})\,\sin(2\,\phi) \;-\; h_{\mathrm{z}}\cos(2\,\phi) \;+\; h_{\mathrm{y}} \tag{16}$$

$$z(p, \theta, \phi) \;=\; (z_{\mathrm{s}}(p, \theta) \;-\; h_{\mathrm{x}}\cos(\gamma/2) \;-\; h_{\mathrm{y}})\,\cos(2\,\phi) \;-\; h_{\mathrm{z}}\sin(2\,\phi) \;+\; h_{\mathrm{z}} \tag{17}$$
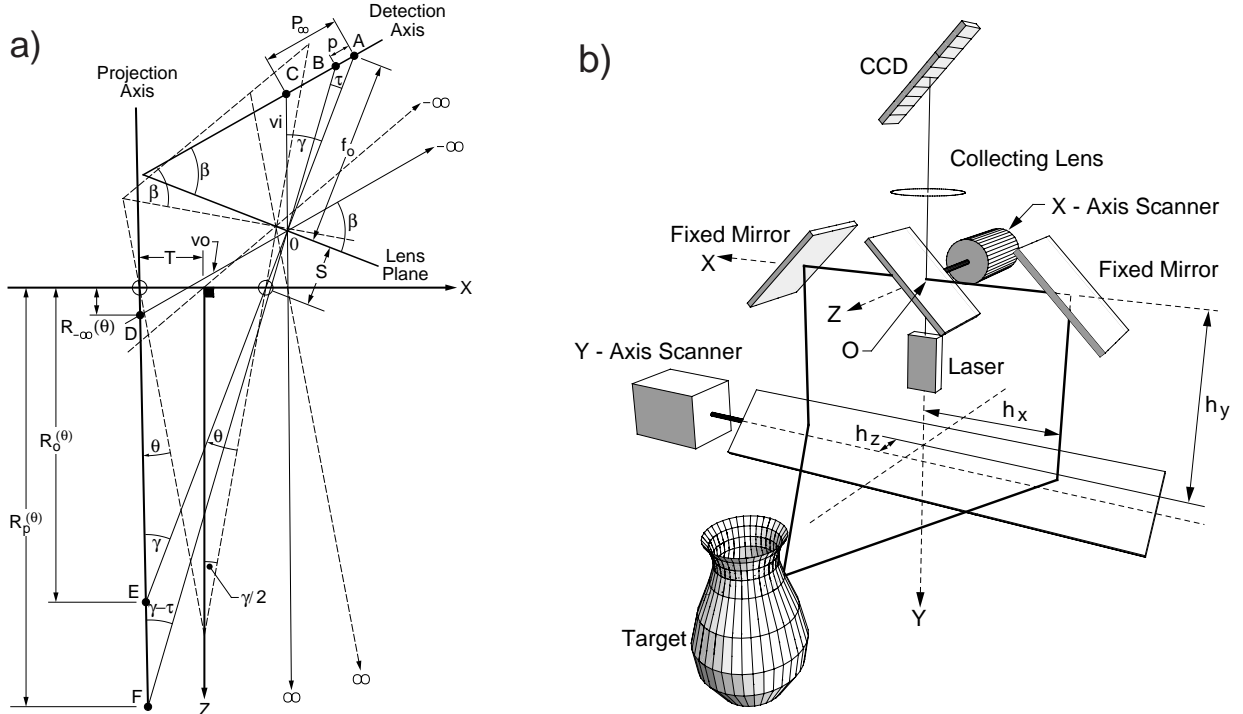
6

Figure 6: Optical arrangement: (a) geometry un-folded along the x-axis scanner, (b) schematic representation of the dual-axis case.

where the coordinate pair $x_{\mathrm{s}}(p,\theta), z_{\mathrm{s}}(p,\theta)$ is the position of a point that would be measured with a range camera having only a single scan axis, i.e., (9)-(10) and ϕ is the mechanical angle of the y-axis scanner. These analytical equations are the projective transformation equations of the synchronized geometry in a rectangular coordinate system and for the dual scan axis case. They form the basis for the derivation of the design tools and calibration method presented in the following section.

4   Description of the Calibration Procedure

4.1   Expected Spatial Precision

The equations that describe the geometry of the camera are used as design tools to characterize the spatial precision. The application of the law of propagation of errors to (15)-(17) is used to estimate the precision as a function of the standard deviation associated to the measurement of (p,θ,ϕ). Another method is the actual calculation of the joint density function. This method, although numerically complex, allows for a full characterization of the three random variables $\mathbf{x}$, $\mathbf{y}$, and $\mathbf{z}$ taken jointly. For the purpose of this design, such a level of sophistication is not required. The law of propagation of errors is sufficient.

This range camera uses two galvanometer to drive each mirror. The pointing precision was measured[4] between 15 m and 47 m and the worst case $\sigma_\theta \simeq \sigma_\phi$ for an optical angle of 30° was about 60 μrad. The measurement of p is in practice limited by the laser speckle impinging on the position detector. Baribeau and Rioux[6] predicted that such noise behaves like a Gaussian process and the estimated fluctuation of p determined by that noise is approximately

$$\sigma_p \;=\; \frac{1}{\sqrt{2\pi}}\,\frac{\lambda\,f_0}{D\,\cos(\beta)} \tag{18}$$

where λ is the wavelength of the laser source and D is the lens diameter. In a well-designed system, when enough light is collected from the scene, the effect of the noise generated in the electronic circuits and the quantization noise of the
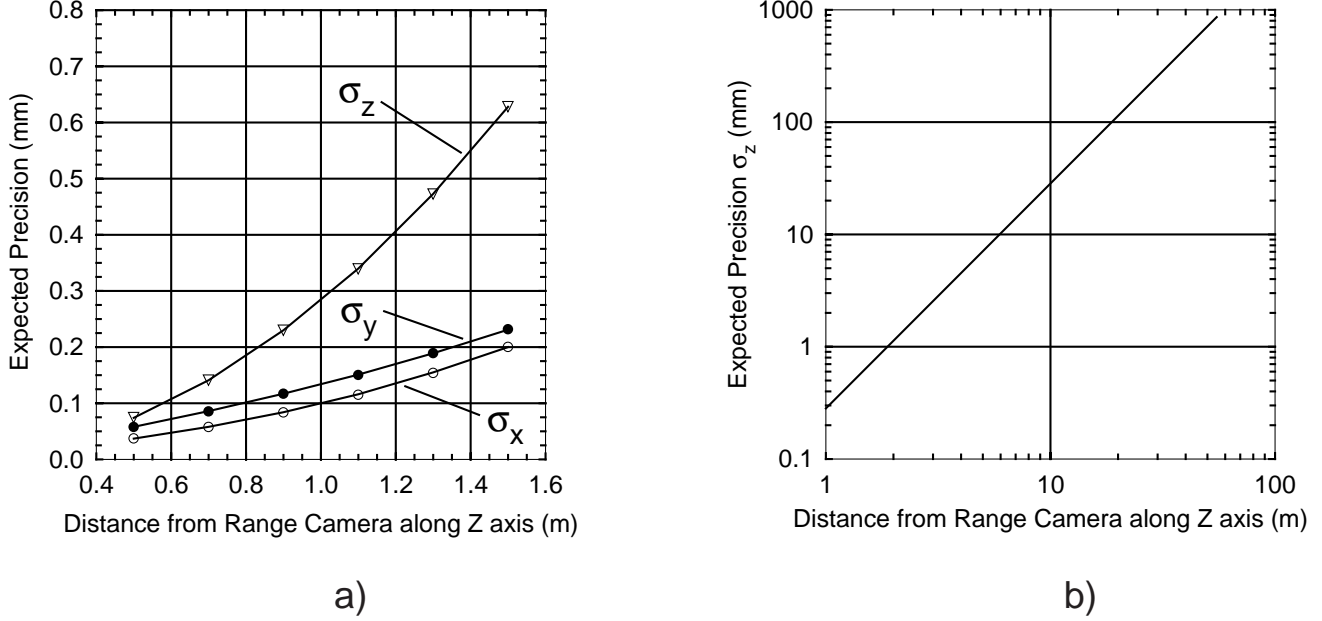
a)

b)

Figure 7: Expected range camera precision $\sigma_\theta = 60~\mu\mathrm{rad}$, $\sigma_\phi = 60~\mu\mathrm{rad}$, $\sigma_p = 3.1~\mu\mathrm{m}$: (a) close-range, (b) far-range.

peak detector on the measurement of p are swamped by speckle noise. With the current camera design the predicted value is $\sigma_p \simeq 3.1~\mu\mathrm{m}$.

Assuming the functions $x = f(p, \theta, \phi)$, $y = g(p, \theta, \phi)$, and $z = h(p, \theta, \phi)$ have no sudden jumps in the domain around a mean value $\overline{p}$, $\overline{\theta}$, and $\overline{\phi}$ allows estimation of the means $(\overline{x}, \overline{y}, \overline{z})$ and the variances $(\sigma_x^2, \sigma_y^2, \sigma_z^2)$ in terms of the mean, variance, and covariance of the random variables $\mathbf{p}$, Θ, and Φ. The analysis of the optical arrangement together with the fact that the errors associated with the physical measurement of p, θ, and ϕ are Gaussian random processes and are loosely related leads one to assume that they are uncorrelated. Therefore, the law of propagation of errors gives

$$\sigma_x^2 \simeq \left(\frac{\partial f}{\partial p}\right)^2 \sigma_p^2 + \left(\frac{\partial f}{\partial \theta}\right)^2 \sigma_\theta^2 + \left(\frac{\partial f}{\partial \phi}\right)^2 \sigma_\phi^2 \tag{19}$$

$$\sigma_y^2 \simeq \left(\frac{\partial g}{\partial p}\right)^2 \sigma_p^2 + \left(\frac{\partial g}{\partial \theta}\right)^2 \sigma_\theta^2 + \left(\frac{\partial g}{\partial \phi}\right)^2 \sigma_\phi^2 \tag{20}$$

$$\sigma_z^2 \simeq \left(\frac{\partial h}{\partial p}\right)^2 \sigma_p^2 + \left(\frac{\partial h}{\partial \theta}\right)^2 \sigma_\theta^2 + \left(\frac{\partial h}{\partial \phi}\right)^2 \sigma_\phi^2 \tag{21}$$

where the functions f, g, and h and their derivatives are evaluated at $p = \overline{p}$, $\theta = \overline{\theta}$, and $\phi = \overline{\phi}$, and σ_p^2, σ_θ^2, and σ_ϕ^2 are the variances of the laser spot detection and the position of the scan mirrors, respectively. Figure 7a provides a graph of the precision predicted by the equations above. At close-range, i.e., 0.5 m to 1.5 m, the maximal value of the (x, y, z) precision in the field of view was plotted against the distance from the camera, Z. The distances are measured from the exit window of the camera. Figure 7b shows only σ_z for distances between 1 m and 100 m.

4.2 Proposed Calibration Method

For this project, an extension of the method presented by Beraldin et al.[5] is used to calibrate the range camera. A calibration bar is adequate to calibrate 3-D volumes in the order of 1 m^3. Any volumes larger than that require a very large calibration bar and a careful setup. A two-step methodology is proposed to alleviate the shortcomings of that method. In the first step, the close-range volume (from 0.5 m to 1.5 m) is calibrated using a flat glass plate composed of an array of targets. This plate is made up of evenly spaced targets on a grid of 5×7. The center of each target was previously measured with a coordinate measuring machine (CMM). The target-background contrast should be high.

8

The target array is positioned at known locations in the field of view of the range camera using a precise linear stage. Here, a large number of targets is used in this region because it is where the camera has its highest range precision. In the second step, it is proposed to use a smaller number of targets (the number of targets is affected by the number of parameters in the model) positioned at distances greater than 1.5 m with the help of an accurate theodolite and electronic distance measuring device. Beyond 10 m, these instruments have angular and distance measuring accuracies 10 times better than this range camera though they have very low measurement rate compared to the 18 000 samples per second of the present system. Once the registered range and intensity images have been acquired for all the targets, the edges of those targets are extracted to sub-pixel accuracy using a moment preserving algorithm. The center of each target (in terms of the coordinates (p, θ, ϕ)) is then determined by fitting an ellipse to the edge points. An iterative nonlinear simultaneous least-squares adjustment method extracts the internal and external parameters of the camera model, i.e., (15)-(17).

To remove most residual systematic errors from the calibration, distortion parameters on (p, θ, ϕ) were included in the model. Equations (15)-(17) require that θ and ϕ be in angular units and p in unit of length. Unfortunately, this is not the case. The angular position of the mirrors are given as an output number from an analog-to-digital converter located on the galvanometer controller card. The laser spot position is an interpolated pixel number. Third-order polynomials are included in the model for the mapping of these dimensionless quantities to the proper variables. Twenty parameters must be solved for in the current range camera model.

5   Accuracy Assessment

5.1   Definitions

To establish standardized measures for vision systems performance, terminology for accuracy must be clearly defined. Ideally, a vision system intended for metrology should provide the distribution of repeated measurements taken on well-known objects and fiducial marks, the operating conditions, all pertinent system parameters, and the specific targeted application. Moreover, the vision system should yield dimensional measurements that have symmetric error distributions, free of systematic errors and artifacts. Considering that the requirements and specifications vary greatly from one application to another, characterizing a vision system becomes a non-trivial task[7]. For the purpose of this experiment, the terms resolution, bias, precision, and accuracy will be defined and used in the context of digital range imaging. No attempt has been made to fully characterize the error distributions.

Resolution is the smallest spatial interval that can be displayed. With this range camera, the resolutions of the scanning axes and the spot position detection are each 16 bits. System *bias* is defined as the difference between the mean of the measurement and the true value of some fiducial mark. The true value of a measurement is, however, unknown and the best estimate one could obtain is from using a superior system. Measurements provided by a well-accepted gauging technique such as a CMM serves as a base for comparison. The term *precision* is defined as the degree of conformity among a set of observations of the same quantity. The spread or dispersion of the measurement of that quantity is an indication of precision. When the distribution of the measurements behaves like a Gaussian distribution, the standard deviation σ is used as a measure of precision. For *accuracy*, both bias and precision must be given as measure of system metric performance. No attempt should be made to combine the two numbers into a single number. Obviously, environmental parameters like temperature, atmospheric pressure, humidity, and mechanical stability must be specified. In this experiment, the accuracy was estimated and verified at a temperature of 25°C ±0.5°C.

5.2   Close-Range Calibration and Evaluation

The results for a close-range calibration are reported here. The second step in the calibration procedure will be discussed in a separate paper. The field of view of the camera was digitized to a resolution of 512×512. The calibration was performed by positioning the target array 0.7 m and 1.1 m from the camera. Forty targets or control points were used for the solution (the minimum being seven). The extracted parameters for the model were then applied to the raw data (both range and intensity) obtained for the same target array located at three other locations: 0.9 m, 1.3 m, and 1.5 m. Note that the last two positions of the array are essentially extrapolated data. Positions 1.3 m and 1.5 m could not be used in the solution because the targets were too small. This target array was not specifically designed for this range camera. Future calibrations will not be hindered by these limitations.
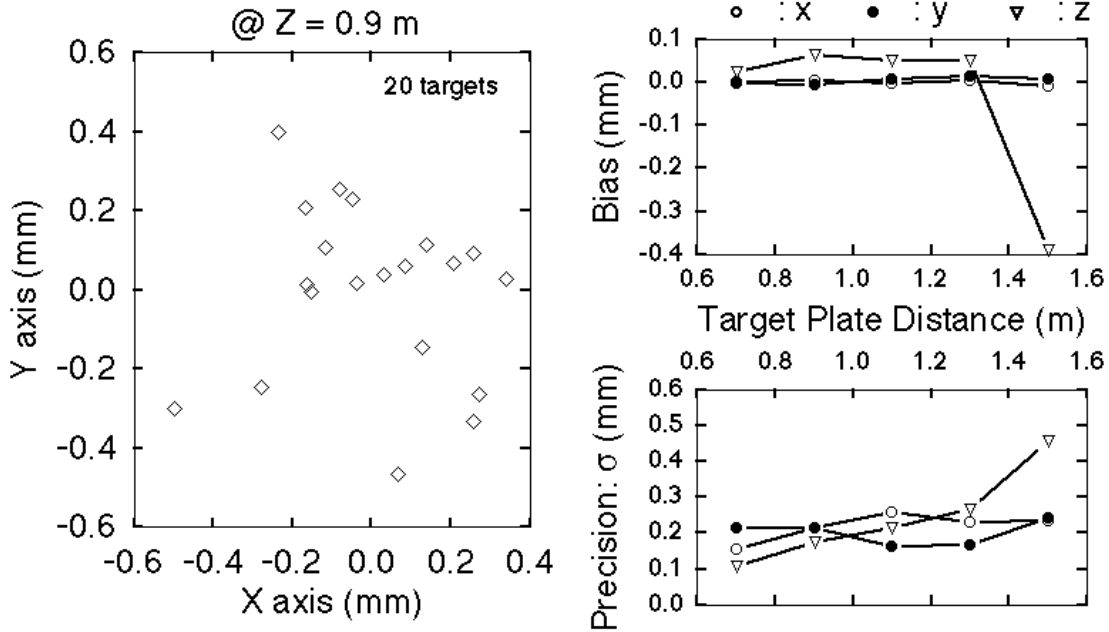
Figure 8: Experimental results obtained for a calibration performed with the target array located at $z = 0.7$ m and $z = 1.1$ m. Left, scatter plot of target positioning error for $z = 0.9$ m. Upper right, bias; Lower right, $\sigma_x, \sigma_y, \sigma_z$ for 100 targets at various distances from camera.

The center of each target (in terms of the coordinates (p, θ, ϕ)) was also determined by fitting an ellipse to the edge points obtained from a moment preserving algorithm applied to the intensity image. The x, y coordinates were then found with (15)-(17). The bias and precision along the x and y axes were determined by comparison to the values given with the target array certificate. The z component was determined by fitting a planar patch on each target at all five positions of the target array (about 100 targets). The results on the bias and precision are presented in Figure 8.

6 Discussion

The proposed calibration method allows for a rapid extraction of the internal and external parameters of the range camera. A target array is positioned at a minimum of two known locations (known spacing between them) and a registered range and intensity image is acquired. It takes less than 1 min. on a personal computer to solve for the camera parameters for a total of 40 targets. The technique was verified for close-range calibration. The experimental results agree with the predicted ones. The z precision is, in fact, better than predicted, except perhaps when measurements are extrapolated outside the calibrated volume. Extrapolation ought to be avoided with the current model of this camera. The increased z precision is explained by the overestimate of σ_p. In practice, it is lower than the value predicted by the speckle noise model. A future experiment will verify the calibration of the remaining volume of measurement with very accurate surveying equipment.

The critical elements of this calibration method are the validity of the model and the number and location of the calibration targets. The model presented in Section 3 resulted from several assumptions related to the nature of the imaging lens and the planarity and location of the scanning mirrors. The scanning mirrors were considered to be infinitely thin and mounted orthogonally. Also, the galvanometer wobble and the diffraction of the laser beam were neglected. Further refinements to the model will come from a better understanding of the distortions created by these assumptions. The next version of the target array will be designed and build according to the requirements of this range camera. Finally, environmental conditions affecting the overall accuracy and other system performance such as automatic extraction of features are either not yet defined or their effects have not been fully determined.

7   Conclusion

This paper introduced a new method for the calibration of a range camera intended for space applications. A model based on the collinearity principle is derived for the synchronized geometry. It is used to extract the internal and external parameters of the range camera with an iterative nonlinear simultaneous least-squares adjustment method. An assessment of the precision and accuracy of this range camera and the proposed calibration method were conducted in a field of view located within a range of 0.5 m to 1.5 m. Experimental results obtained for a close range calibration suggest a precision along the x, y and z axes of 200 μm, 200 μm, and 250 μm, respectively, and a bias of less than 100 μm in all directions. These results are satisfactory for the intended application of this range camera. Although a laser range finder based upon the synchronized scanner approach was considered, other active triangulation geometries with different requirements can be accommodated by a similar analysis and calibration procedure.

The evaluation of the performance of vision systems for metrology is challenging since it is concerned with all aspects of evaluation, i.e., image quality and detection success, and also involves the understanding of all system parameters and how they interact to produce certain results. Rigorous range camera calibration is essential for vision applications, if one wants to speed up the transition of vision systems from laboratory to the space environment or to the factory floor where accurate measurement is required. An important factor is the lack of reliable methods for predicting the performance of a proposed solution for a given application. It is also very difficult to model or predict the performance without a near perfect and stable calibration process.

8   Acknowledgements

References

[1] M. Rioux, "Applications of Digital 3-D Imaging," Canadian Conference on Electrical and Computer Engineering., Ottawa, Sept. 4–6, 37.3.1–37.3.10 (1990).

[2] P.J. Besl, "Range Imaging Sensors," Mach. Vision Applic., 1, 127–152 (1988).

[3] M. Rioux, "Laser Range Finder based on Synchronized Scanners," Appl. Opt., 23, 3837–3844 (1984).

[4] F. Blais, J.-A. Beraldin, M. Rioux, R.A. Couvillon, and S.G. MacLean, "Development of a Real-Time Tracking Laser Range Scanner for Space Applications," Workshop on Computer Vision for Space Applications, Antibes, France, Sept. 22–24 (1993) In Press.

[5] J.-A. Beraldin, R. Baribeau, M. Rioux, F. Blais, and G. Godin, "Model-Based Calibration of a Range Camera", Proc. of 11th IAPR Int. Conf. on Pattern Recognition, The Hague, The Netherlands, Aug. 30–Sept. 3, 163–167, (1992).

[6] R. Baribeau and M. Rioux, "Influence of Speckle on Laser Range Finders," Appl. Opt., 30, 2873–2878 (1991).

[7] S.F. El-Hakim, "Application and Performance Evaluation of a Vision-based Automated Measurement System," Videometrics, SPIE Proceedings, Vol. 1820, 181–195 (1992).

[8] F. Blais, M. Rioux and J.-A. Beraldin, "Practical Considerations for a Design of a High Precision 3-D Laser Scanner System," SPIE Proceedings, Vol. 959, 225–246 (1988).